American Mineralogist, Volume 82, pages 596–606, 1997

Statistical characteristics and origin of oscillatory zoning in crystals

Terje Holten,[1] Bjørn Jamtveit,[1] Paul Meakin,[2] Massimo Cortini,[3] Jon Blundy,[4] and Håkon Austrheim[5]

[1]Department of Geology, University of Oslo, P.O. Box 1047 Blindern, N–0316 Oslo, Norway
[2]Department of Physics, University of Oslo, P.O. Box 1048 Blindern, N–0316 Oslo, Norway
[3]Department of Geophysics, University of Napoli, Largo S. Marcellino 10, 80138 Napoli, Italy
[4]CETSEI, Department of Geology, Bristol University, Wills Memorial Building, Queens Road, BS8 1RJ, Bristol, U.K.
[5]Mineralogical Geological Museum, Sars gate 1, N–0562 Oslo, Norway

Abstract

Complex intracrystalline zoning patterns in hydrothermal garnet and vesuvianite and magmatic plagioclase were analyzed by statistical methods to test for fractal behavior. The zoning data were collected by electron and proton microprobe, and backscattered electron images and polarized micrographs were digitized. The analysis shows that self-affine fractal geometry can be used to characterize the zoning patterns of vesuvianite and some garnet patterns. The range of power-law scaling extended up to two decades. The results from the plagioclase samples were not sufficient to determine whether or not the zoning patterns were self-affine. The measured Hurst exponents are mostly in the range 0.25–0.45, indicating fractal scaling and anti-persistent behavior. This means that an increasing compositional trend in the past favors a decreasing trend in the future and vice versa. No distinct periodic components of the zoning patterns were found.

The influence of environmental changes (external fluctuations) on a simple crystal growth model was investigated by numerical simulations. The concentration at the boundary of a diffusion layer was allowed to vary as a Brownian-motion curve, and the effect of the external fluctuation on diffusion and local growth kinetics was investigated. We conclude that factors operating on scales much larger than the local interface processes are most important in controlling the zonation.

Introduction

Oscillatory zoning in minerals is a common phenomenon (Shore and Fowler 1997), and has been reported from a variety of geological environments. The rich structure represented by such zoning patterns contains potentially valuable information about crystal-growth processes as well as changes in the environment in which the crystals grow. Attempts to explain complex mineral zoning patterns commonly have been based on either of two different assumptions: (1) The zonation is a result of internal crystal growth processes (Haase et al. 1980; Allegre et al. 1981; Simakin 1983; Wang and Merino 1992; Ortoleva 1990; L'Heureux and Fowler 1994), or (2) the zonation mainly reflects changes in the external geological environment during crystal growth (Yardley et al. 1991; Jamtveit et al. 1993; Jamtveit et al. 1995). The first model implies that oscillatory zonation is generated without any external template, i.e., by self-organization. This requires that the geological processes of interest take place far from equilibrium. Nonequilibrium situations result from a large mass or heat flux through or into an open system or by some other means, but in general require some sort of interaction with the environment to drive the system away from a time-invariant state. The second model accounts for oscillatory zonation in a system in which the crystal is near local equilibrium with its environment and the zonation pattern is a direct reflection of changes in the environment. Such changes are commonly ascribed to a variable mass flux through an open system, but also they may reflect fluctuation in variables such as temperature and pressure. In both cases, however, oscillatory zoning represents the response of a local system to some external forcing. In magmatic systems, this forcing may be represented by magma mixing, rapid cooling, or degassing whereas in metamorphic and sedimentary systems the forcing may be related to fluid flow with associated advective transport of mass and heat or fluctuations in the pore-fluid pressure. A priori assumptions about the role of internal vs. external controls on a given mineral zonation pattern are clearly not warranted unless it can be unambiguously demonstrated that fluctuations in the environment (i.e., external forcing) operate on time scales very different from the crystal-growth rate. In our experience this is rarely the case.

In this paper we first analyze the statistical properties of complex zonation patterns from magmatic plagioclase and hydrothermal garnets and vesuvianite by methods well known from the literature on fractal geometry. We

0003–004X/97/0506–0596$05.00

then present a simple growth model and investigate how the zoning pattern responds to various external forces. A comparison is made between the observed patterns and this model.

Fractal geometry

It has recently been suggested that oscillatory-zoning patterns can be described in terms of self-affine fractals (Halden and Hawthorne 1993). Fractal geometry has been applied to a wide range of phenomena in recent years (Mandelbrot 1982; Feder 1988; Meakin 1997). Fractals are characterized by a fractal dimension, *D*, which is a measure of how much space the fractal fills at different length scales. A fractal that scales equally in all directions is called self-similar. A fractal that scales differently in different directions is called self-affine. This is often the case when the directions have different physical dimensions for instance a spatial dimension and time.

A 1 + 1 dimensional self-affine fractal, *y(x)*, is statistically invariant under the transformation

$$x \to \lambda x,$$
$$y \to \lambda^H y \tag{1}$$

where H is called the Hurst exponent (or roughness exponent). The absolute vertical height difference δy between pairs of points separated by a distance δx in the x direction scales on the average as $\langle \delta y \rangle \sim (\delta x)^H$ ($\langle \cdots \rangle$ denotes average). The analysis of self-affine fractals using methods that are better suited to self-similar fractals has caused considerable confusion in the literature. If a self-affine, 1 + 1 dimensional fractal is analyzed by ''box-counting'' (a method commonly used for self-similar fractals) a fractal dimensionality of $D = 2 - H$ (the local dimension) will be found on short length scales where $\langle \delta y \gg \delta x \rangle$ and a fractal dimension of one will be found on long length scales where $\langle \delta y \rangle \ll \langle \delta x \rangle$ (Mandelbrot 1985). Because of the crossover from $D = 2 - H$ on short length scales to $D = 1$ on long length scales the results will be unreliable in the short length scale regime, unless $\langle \delta y \rangle \gg \langle \delta x \rangle$, and will be misleading in the long length scale regime where a Hurst exponent of one is obtained if it is assumed that $H = 2 - D$. The position of the crossover can be changed by rescaling the y coordinates, and if the curve *y(x)* is amplified sufficiently the condition can be satisfied for all values of x. However, this rescaling is not usually done, and this approach to measuring the Hurst exponent is not recommended. Mineral zonation patterns cannot be self-similar because distance and composition have different dimensions.

Brownian motion is an example of a self-affine fractal time series. Brownian motion can be defined as the position of a particle with independent Gaussian-random increments as a function of time. Fractional Brownian motion (fBm) (Feder 1988) is a generalization of ordinary Brownian motion. For fBm, the position $B_H(t)$ scales as function of time, t, as $\lambda^H B_H(t) \equiv B_H(\lambda t)$, where ''$\equiv$'' means ''statistically equivalent to.'' For ordinary Brownian motion, $H = \frac{1}{2}$. In Figure 1, fBm was generated with the Fourier-filtering method (Peitgen and Saupe 1988) for $H = 0.1$, 0.5, and 0.9. Smaller H values lead to fractals that look rougher and have sharp peaks. In the limit $H \to 0$, the mean vertical fluctuation λy is independent of the horizontal resolution, λx. A Hurst exponent $H > 0.5$ means that the time record is persistent: An increasing or decreasing trend in the past favors an increasing or decreasing trend in the future. The increments are positively correlated. If $H < 0.5$, the record is anti-persistent: An increasing or decreasing trend in the past favors a decreasing or increasing trend in the future.

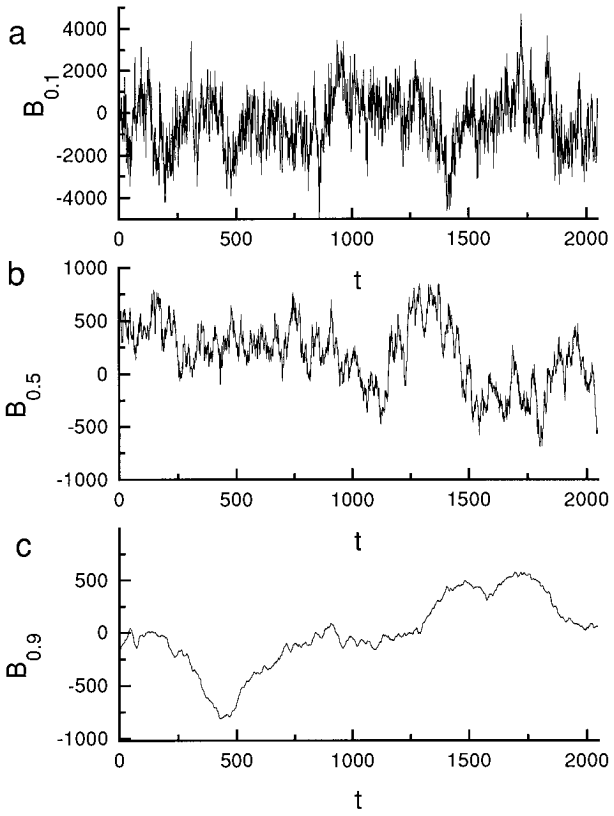

Figure 1. Fractional Brownian motion generated by the Fourier-filtering method. The position $B_H(t)$ of a particle is shown as function of time t. The curves were generated with (**a**) $H = 0.1$, (**b**) $H = 0.5$, and (**c**) $H = 0.9$. These are examples of self-affine fractals with a (local) fractal dimension given by $D = 2 - H$.

The width

Many different methods have been used to measure the Hurst exponent describing single valued functions *y(x)*. The width w of a function *y(x)* is defined as

$$w(l) = [\langle y^2(x) \rangle_l - \langle y(x) \rangle_l^2]^{1/2}, \tag{2}$$

where $\langle \ldots \rangle^l$ denotes an average over all sections (x_0 to $x_0 + l$) with a length l. The width w scales as

$$w(l) \approx l^H \tag{3}$$

for self-affine fractals. This is a common method for measuring the Hurst exponent (roughness exponent) of rough surfaces (Meakin 1997).

The power spectrum

Another method for analyzing time series is the power spectrum (Voss 1986; Feder 1988), used by Halden and Hawthorne (1993) in their analysis of $ZrSiO_4$ zonation. The exponent β of the power spectrum $G(f) \approx 1/f^{\beta}$ can be related to the Hurst exponent, H, by $\beta = 2H + 1$. With few measurements, power spectra have high standard deviations and the local slope may change rapidly. A high degree of averaging is needed to obtain power spectra with a low noise level.

Interpretation of zoning patterns

By measuring the concentration, c_s, of some component in a mineral as a function of position x, from the core, a zoning pattern is obtained. As solid-phase diffusion is often too slow to change the zonation even on times scales of 100 Ma, zoning patterns commonly represent the variation of composition immediately after crystallization. If the growth velocity were constant during growth, the zoning pattern would be analogous to a time series. It is probably unrealistic to assume that the growth velocity is constant for the whole time span of crystal growth in real geological systems. Zoning patterns can then be interpreted as time series that are distorted by a non-constant velocity, $V(t)$. The time t relative to the time of nucleation can be calculated as a function of position x as

$$t(x) = \int_0^x \frac{dx'}{V[c_0(x')]} \tag{4}$$

where c_0 is the interface concentration of the component in the fluid. The transformation of a zoning pattern $c_s(x)$ to a time series $c_s(t)$ can be performed if experimental data of the growth rate $V(c_0,T)$ are available and the dependence of c_0 on c_s is uniquely known. Additional assumptions are needed: a constant crystallization temperature T, pressure, and concentration of other fluid components affecting the growth rate. Sometimes, crystal growth is interrupted by dissolution. In the case of unrecognized dissolution, the interpretation of the zoning pattern in terms of a time series is increasingly unrealistic since part of the time series is lost.

The main difference between zoning patterns and rough surfaces is that zoning patterns are always bounded. The molar fractions are always limited by zero and one, and in practice the range of molar fractions is often much narrower. On the other hand, if a 1 + 1 dimensional fractal surface $y(x)$ is traced along the x direction starting with $y(0) = 0$, then $\langle|y(x)|\rangle \to \infty$ as $x \to \infty$. Therefore zoning patterns cannot be self-affine for concentration scales greater than concentration range Δ (the difference between the maximum and minimum concentrations). An effective Hurst exponent close to zero will be measured in this region. The crossover can be described in terms of a function $f(x)$ and a crossover length l^*. The width w follows the relationship

$$w(l) = l^H f(l/l^*), \tag{5}$$

$$f(x) = \begin{cases} c' & x \ll 1 \\ c'x^{-H} & x \gg 1 \end{cases} \tag{6}$$

where $c' \cong (l^*)^{-H}\,\Delta$ is a constant. Zoning patterns can furthermore be described by single-valued functions, unlike rough surfaces, which may have overhangs.

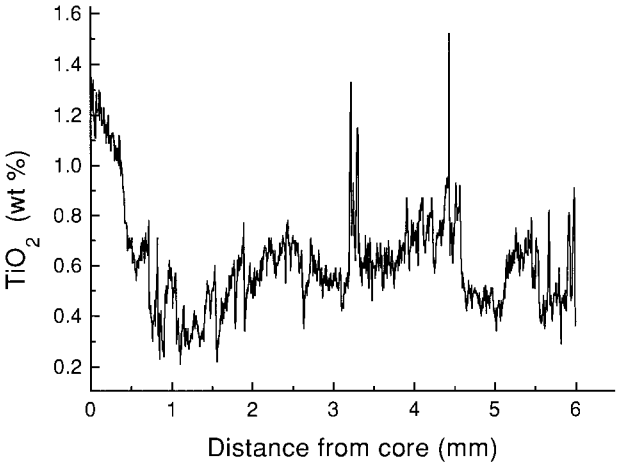

Figure 2. TiO_2 content in vesuvianite crystal V2 measured by electron microprobe.

Fractal analysis of samples

The sample descriptions and geological settings are described in Appendix 1. The details of the image analysis and EMP and PIXE measurements are described in Appendix 2. In those cases in which two independent measurements were made on the same crystal they are distinguished by the letters a and b. The sample-to-sample statistical errors of all experimentally measured Hurst exponents are similar, about 0.05.

Vesuvianite profiles

The Ti content of two hydrothermal vesuvianite crystals, V1 and V2, was measured by electron microprobe. Ti substitutes for Al, which is in octahedral coordination with O atoms. The TiO_2 content in these crystals varies between 0.2 and 2.0 wt%. Figure 2 shows the very irregular Ti profile of the vesuvianite crystal shown in Figure 3 (sample V2). The width of the profiles were measured (Fig. 4), by inserting $c_s(x) = y(x)$ in Equation 2. The results from V1 and V2 (Table 1) showed power-law behavior over about two orders of magnitude, giving Hurst exponents (Eq. 3) of about 0.26 and 0.29, respectively (Fig. 4). These results show that the profiles can be described in terms of self-affine fractal geometry over a significant range of length scales. V2 was also photographed in a cross-polarized light microscope. The photograph (Fig. 3) shows alternating light and dark bands.

FIGURE 3. Cross-polarized light photograph of vesuvianite crystal V2. The horizontal scale is 2.5 mm.

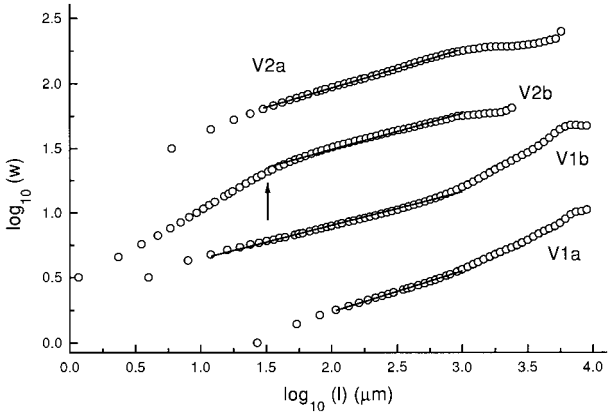

FIGURE 4. The width, *w*, as a function of the length *l* for TiO_2 content in vesuvianite (circles). V1a and V1b are two independent EMP measurements of the same crystal. V2a and V2b are EMP and cross-polarized photograph measurements of the same crystal. The lines show the best fits to Equation 3 in the ranges in which the data were fitted. The vertical scale is arbitrary. The arrow shows the thickness of the thin section 30 μm.

The intensity of these bands is strongly correlated with the Ti concentration. The photograph was digitized, and the width of the resulting zoning pattern (sample V2b) was measured (Fig. 4). By fitting this profile in the same range of length scales as V2a, a similar Hurst exponent of 0.28 was obtained. For V2b, there is a clear crossover to $H \approx 0.60$ at smaller length scales. This is probably due to the lack of spatial resolution at distances less than the thickness of the thin section (30 μm). Two independent spectrometers were used during the EMP measurement of the Ti content of V2. The measurements did not deviate significantly from each other. The *H* values measured from all zoning patterns of V1 and V2 are equal within the estimated error (Table 1). This consistency provides further evidence of a self-affine geometry at length scales ranging from about 30 μm to 1 mm.

Garnet profiles

The analyzed garnets originated in contact aureoles in the Permian Oslo Rift, South Norway (see Appendix 1). The garnets are part of a solid-solution series from andradite ($Ca_3Fe_2Si_3O_{12}$) to grossular ($Ca_3Al_2Si_3O_{12}$). Distinct bands are evident in the backscattered-electron (BSE) images (Fig. 5). The widths of three digitized BSE images and seven EMP zoning profiles (Fig. 6) were measured (Fig. 7, Table 2). Sample SK24 was also analyzed by the power-spectrum method. The width measurements resulted in Hurst exponents in the range 0.14–0.55. Zoning profiles with few data (~150) tend to give lower Hurst exponents and are not reliable. The longer series show apparent power-law scaling over 1–2 orders of magnitude in length scale. Some samples (e.g., GB and GB13) show clear crossovers from high Hurst exponents on short length scales to low Hurst exponents on longer length scales. The most convincing fractal behavior is shown by samples SK24 and K92−2, which show linear trends over 1.5–2 orders of magnitude. One problem apparent from the analysis of K92−2 is that the electron microprobe zonation profile and the profile obtained from image processing resulted in significantly different Hurst exponents (0.55 and 0.40, respectively). This is probably caused by somewhat greater experimental noise in the latter case.

TABLE 1. The effective Hurst exponent *H* measured from the width *w*(*l*) of zoning patterns of Ti content of vesuvianite

Sample	Ti (wt%)	*H*	$\log_{10}L_{min}$	$\log_{10}L_{max}$	*n*	Analysis
V1a	0.34–1.96	0.31	2.0	3.0	348	EMP
V1b	0.28–1.82	0.26	1.0	3.0	2368	EMP
V2a	0.21–1.52	0.29	1.5	3.0	999	EMP
V2b		0.28	1.5	3.0	2099	photo

Note: The analysis method is either electron microprobe (EMP) or digitized photgraphs (photo). *n* is the number of measurement points, which is equal to the number of pixels for digitized photographs. The results were fitted in the range l_{min}–l_{max} (measured in micrometers). This was the largest range for which a reasonable fit to a power law could be obtained. The statistical error in the *H* estimate is about 0.05.

FIGURE 5. Backscattered electron (BSE) image of garnet crystal K92−2. The andradite-rich sections are light, whereas the grossular-rich sections are dark. The horizontal scale is 9 mm.

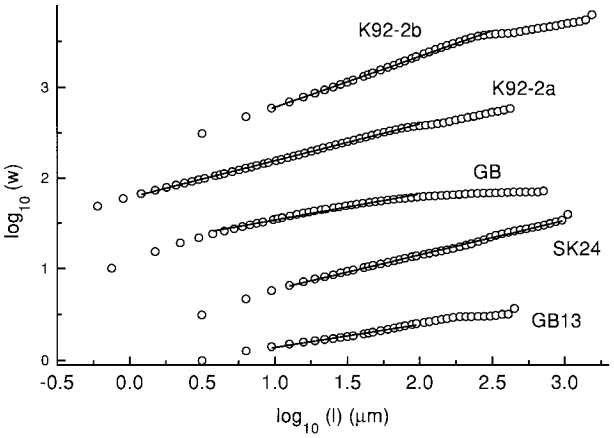

FIGURE 7. The width *w(l)* of zoning patterns of garnets. The zonation was measured by EMP [SK24 (Fig. 6), GB13 (Fig. 6), K92-2b and B19] and by digitizing BSE images [K92-2a (Fig. 5) and GB]. The results were shifted upward on the *y* axis for illustration purposes.

Plagioclase profiles

The zoning patterns of two plagioclase crystals, SS40 (from the Cerro Galan caldera) and SH80-D (from Mount St. Helens), were measured by EMP and PIXE, respectively (see Appendix 1 for details). The patterns show irregular behavior (Figs. 8–9). The results from the width measurements are shown in Figure 10 and Table 3. The fractal scaling of the plagioclase data is less convincing than those of the vesuvianite and some of the garnets. The slope in the log-log plot of the SS40 result decreases monotonically as the length scale *l* increases. The result from sample SH80-D may be fitted by a power law, but the data are not sufficient to establish fractal scaling. The results suggest a crossover between different regimes rather than a simple fractal scaling.

The zoning pattern of sample SS40 was transformed to a time series by using experimental data and Equation 4. The fit based on a growth model studied by L'Heureux (1993) to the experimental data of Kirkpatrick et al. (1979) was used to estimate the growth velocity. The temperature was estimated as the solidus temperature (Muan 1979) of the average composition $An_{34,}$ T = 1505 K. This calculation assumes that the melt consists only of the components albite and anorthite.

However, it is not expected that the statistical behavior

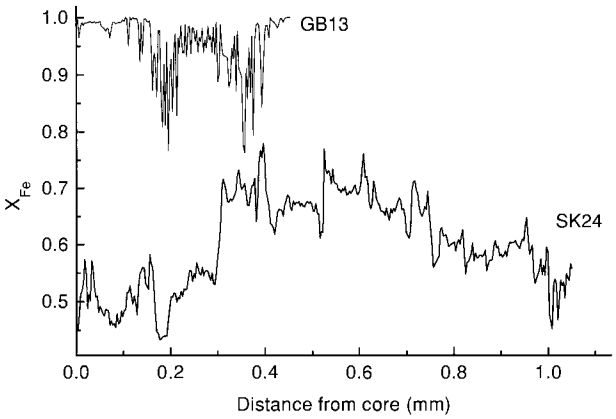

FIGURE 6. Electron microprobe (EMP) measurements of the X_{Fe} content of garnets SK24 and GB13.

TABLE 2. The effective Hurst exponent *H* measured from zoning patterns of X_{Fe} content in garnets

Sample	X_{Fe}	*H*	$\log_{10}L_{min}$	$\log_{10}L_{max}$	*n*	Analysis	Method
SK24	0.43–0.78	0.38	1.0	3.0	341	EMP	*w*(*l*)
SK24	0.43–0.78	0.44	0.8	1.8	341	EMP	PS
B19	0.34–0.60	0.23	1.0	2.0	162	EMP	*w*(*l*)
N6	0.71–1.00	0.33	1.0	2.5	204	EMP	*w*(*l*)
Grua1	0.72–1.00	0.40	1.0	2.0	174	EMP	*w*(*l*)
K92-5	0.57–1.00	0.14	1.0	2.0	138	EMP	*w*(*l*)
GB13	0.76–1.00	0.25	1.0	2.0	147	EMP	*w*(*l*)
N25		0.25	1.0	2.0	1528	BSE	*w*(*l*)
K92-2a		0.40	0.0	2.0	1525	BSE	*w*(*l*)
K92-2b	0.65–0.99	0.55	1.0	2.5	501	EMP	*w*(*l*)
GB		0.29	0.5	2.0	971	BSE	*w*(*l*)

Note: The width [*w*(*l*)] and power spectra (PS) were used. X_{Fe} was measured by electron microprobe (EMP) or by measuring the light intensity in a backscattered electron (BSE) image; the range of composition is shown for EMP. The results were fitted in the range l_{min}–l_{max} (measured in micrometers). *n* is the number of measurement points.

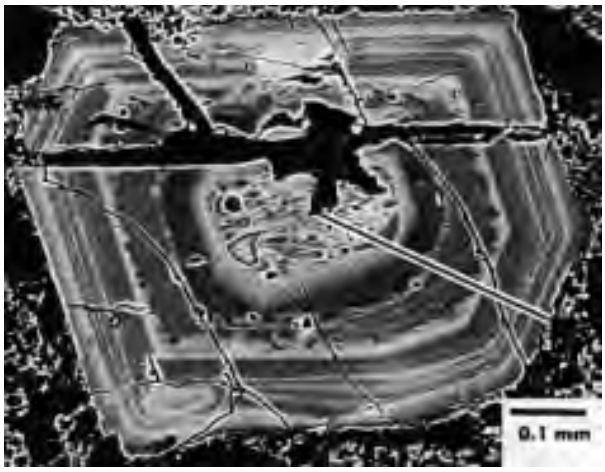

FIGURE 8. BSE photograph of plagioclase crystal SH80-D. The line shows the location of the PIXE measurement.

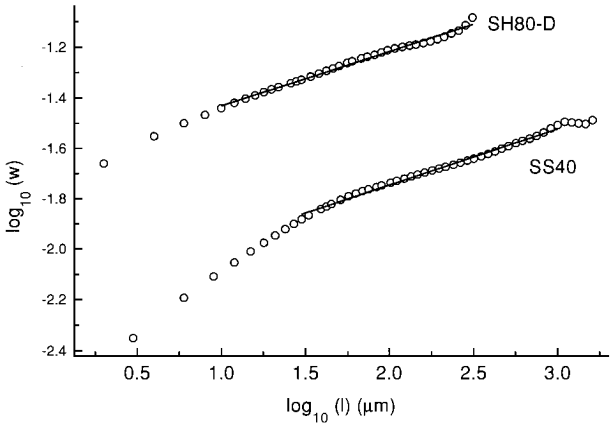

FIGURE 10. The width *w(l)* of the zonation of plagioclase samples SH80-D and SS40. The vertical scale is arbitrary.

of the zoning pattern (i.e., *H*) is sensitive to the actual melt composition. The width measurements of this time series look almost exactly like Figure 10, with a trend toward a constantly decreasing slope with increasing time. The value of *H* is about 0.19 when measured between one and ten years. The total time required for crystal growth is roughly estimated to be 110 years.

SIMULATIONS

A simple one-dimensional model was constructed to investigate the effect of external stochastic forcing on diffusion and local growth kinetics. As the fluid composition can vary on time scales that are many orders of magnitude less than the duration of crystal growth, these changes can be thought of as some kind of external fluctuation in hydrothermal systems. Changes of other parameters affecting growth, like temperature and pressure, can also be thought of in terms of fluctuations: these parameters are assumed to be constant in the subsequent discussion. A variable concentration was input as an external fluctuation at the end of a diffusion layer, which was maintained at a distance *L* from the solid-liquid interface (Fig. 11). It is convenient to let the reference frame move with the solid-liquid interface as crystal growth proceeds, thus keeping the solid-liquid interface at the position $x = 0$. The evolution of the mole fraction *c(x,t)* of a component of the solid due to diffusion and the moving interface is then given by (Lasaga 1982)

$$\frac{\partial c}{\partial t} = D\frac{\partial^2 c}{\partial x^2} + V\frac{\partial c}{\partial x}, \tag{7}$$

where *D* is the diffusion coefficient, *V* is the crystal growth velocity, and *t* is time. The external noise was modeled as ordinary Brownian motion $B_{1/2}(t)$. The noise was scaled to the range 0–1 after generation by the Fourier-filtering method. The nature of real external fluctuations is unknown, so the most simple assumption, that the fluctuation has a Hurst exponent $H = 0.5$ (i.e., statistically independent increments) and is artificially bounded, was made to examine the response of the zoning pattern to the external noise. The boundary condition at $x = L$ is then $c(L,t) = B_{1/2}(t)$, where $0 \leq B_{1/2}(t) \leq 1$. The composition of the solid, c_s, is related to the composition near the solid-liquid interface $c_0 = c(0,t)$ through $c_s = Kc_0$, where *K* is the solid-liquid partition coefficient. Generally, the effective partition coefficient *K* depends on c_0 and other parameters. Here it was assumed that *K* is con-

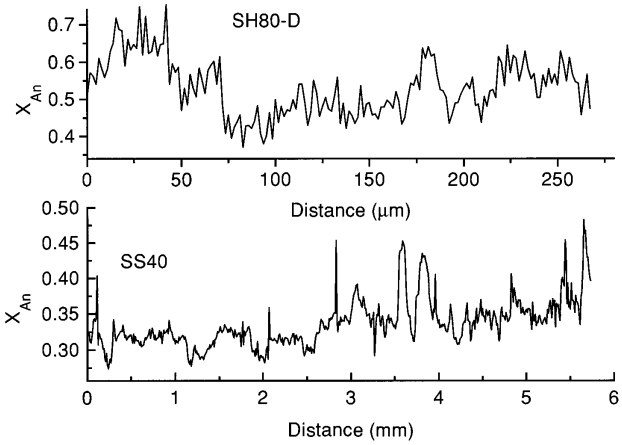

FIGURE 9. The composition X_{An} of plagioclase crystals SH80-D (top) and SS40 (bottom) measured by PIXE and EMP, respectively.

TABLE 3. The effective Hurst exponent *H* measured from the width *w(l)* of zoning patterns of X_{An} content in plagioclase

Sample	X_{An}	*H*	$\log_{10}l_{min}$	$\log_{10}l_{max}$	*n*	Analysis
SH80-D	0.37–0.75	0.21	1.0	2.4	172	PIXE
SS40	0.27–0.48	0.22	1.5	3.0	574	EMP

Note: The results were fitted in the range l_{min}–l_{max} (measured in micrometers). *n* is the number of measurement points.

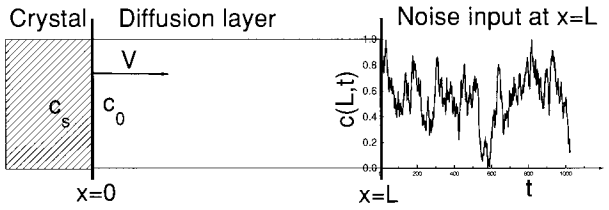

FIGURE 11. Schematic diagram illustrating the simulations. The origin of the coordinate system ($x = 0$) is placed at the solid-fluid interface. Brownian noise $B_{1/2}(t)$ is input at $x = L$.

stant. Continuity of the particle flux at $x = 0$ requires that (Lasaga 1982)

$$D\frac{\partial c}{\partial x}\bigg|_0 + (1 - K)Vc(0, t) = 0. \quad (8)$$

Initially, the concentration is zero in the region $0 \leq x \leq L$, $c(x,0) = 0$. L'heureux (1993) showed that for constant $K \geq 1$, oscillating patterns are not possible in the absence of external forcing. Since realistic K values for hydrothermal systems are commonly in the range 100–1000 (at least for major crystal-forming components), our study is restricted to $K \geq 1$, which also applies to many melt-mineral systems. The position x and time t were made dimensionless by defining $x = xV/D$ and $t = V^2t/D$. An implicit finite-difference scheme with central differences was used in the simulation. An iterative method was used, as described by L'Heureux (1993), with the same relaxation factor (0.50) and tolerance (10^{-6}). The number of time steps used in the simulations was 2^{20} ($\sim 10^6$). Zoning profiles were calculated by plotting c_s against $x = \int_0^t V(t')dt'$.

Pure diffusion

The special case in which D, L, and V are constant was studied, and the zoning profiles $c_s(x)$ were analyzed by measuring $w(l)$. The only section of the zoning pattern analyzed was the portion after twice the time when $c(0,t) > 0$ (in practice 10^{-3}) was analyzed. At length scales smaller than a correlation length ξ the zonation pattern is smooth and nonfractal. At length scales much larger than ξ, the noise pattern is unaffected by diffusion (Fig. 12). Figure 13 shows the width measurement of a zoning pattern obtained with $L = D/V$ and $K = 1$. Here $\xi \approx L$. The results were insensitive to K. For length scales $l \ll L$, $H \approx 1.0$, whereas $H \approx 0.5$ if $l \gg L$. In other words, ξ is the maximum spatial extent of the smoothing of the noise signal (Fig. 12). The correlation length is independent of the nature of the noise; the noise is only affected at length scales $l \leq \xi$.

The general dependence of ξ on D, L, and V can be found from theoretical arguments. There are two length scales in the model; the distance between the noise source and the interface, L, and the diffusion length D/V. If $D/V \ll L$, the time t_0 needed for the noise to reach $x = 0$ is on the order of L/V because the evolution of the concentration profile due to diffusion will be much slower than

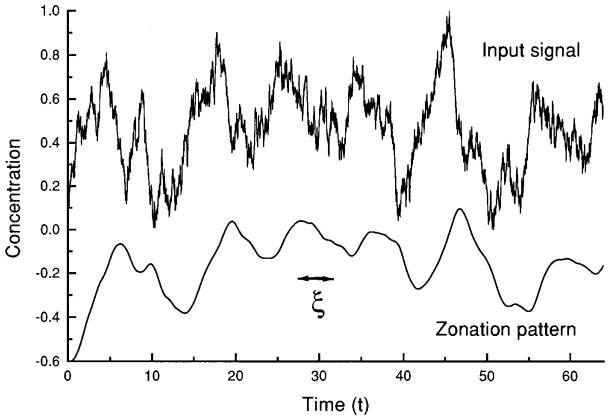

FIGURE 12. Diagram illustrating the concept of the correlation length, ξ, which describes the extent to which the input signal becomes smoother. The input signal $c(L,t)$ reaches the solid-fluid interface after a time t_0. The zonation pattern $c_s(x)$ is similar to $c_s(t)$ (shown) as V is constant. The time scale is arbitrary, the output signal has been shifted downward on the y axis by 0.6 for illustration purposes. This simulation was performed with $L = D/V$ and $K = 1$.

the movement due to the moving interface. The smoothing of the noise due to diffusion during the same time will be $\xi \cong \sqrt{Dt_0} = \sqrt{DL/V}$. On the other hand, if $D/V >> L$, the time needed for the noise to reach $x = 0$ due to diffusion is $t_0 \; L^2/D$. The correlation length ξ is approximately equal to the distance $Vt_0 = VL^2/D$ moved by the solid-liquid interface during the same period of time. The limiting laws are then

$$\xi \simeq \sqrt{\frac{DL}{V}}, \qquad VL/D \gg 1 \quad (9)$$

$$\xi \simeq L, \qquad VL/D \simeq 1 \quad (10)$$

$$\xi \simeq \frac{VL^2}{D}, \qquad VL/D \ll 1 \quad (11)$$

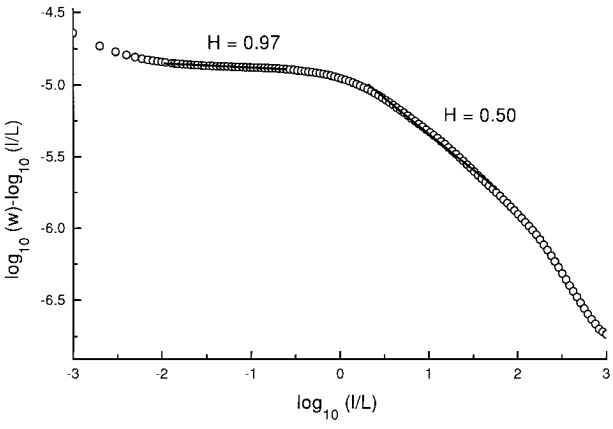

FIGURE 13. The width $w(l)$ measured from the resulting zonation pattern from a numerical simulation with $L = D/V$ and $K = 1$. In this plot log 10 (l/L) has been subtracted from $\log_{10}$ (W) on the y axis to show the crossover more clearly.

"≃" should be interpreted as "has the same order of magnitude as". These equations were confirmed by numerical simulations. In the $D \to 0$ and $D \to \infty$ limits, $\xi \to 0$. An upper limit for ξ for growth from hydrothermal solutions can be found by inserting limits on L, D, and V: $V_{max}L_{max}/D_{min} \simeq (10^{-8}$ m/s $\times\ 10^{-4}$ m$)/10^{-9}$m^2/s $= 10^{-3}$. Inserting these values into Equation 11 gives $\xi \leq 10^{-7}$m . This means that the zoning profiles and input signals are equal in practice since ξ is smaller than the resolution of the measurements. According to this model, the effect of diffusion on an externally imposed zoning profile cannot be observed in open hydrothermal systems. For growth in a porous medium, D must be replaced by the effective diffusion coefficient $D_{eff} = \phi\ \tau^{-2}D$, (Appelo and Postma 1993) where Ø is the porosity and τ is the tortousity (the ratio of the effective transport length to the linear extent). In a porous medium under low porosity, convection-free conditions, and with a source of noise located further away from the mineral, the effect of diffusion on the externally imposed template may be observed. The result will be similar to Figure 13 with L replaced by ξ. For growth in a melt, $V_{max}L_{max}/D_{min} \cong 10^{-11}$m/s $\times\ 10^{-4}$m/10^{-12}m^2/s $= 10^{-3}$, which gives an upper limit $\xi\ 10^{-7}$ m, which is again below detection limits.

Interface-concentration–dependent velocity

The growth rate is generally a function of the concentration at the solid-liquid interface. A reasonable assumption is that V increases monotonically with c_0. The effects on zonation were studed for an nth-order power law $V = V_0c(t)n$, with $0 \leq n \leq 3$ (setting the equilibrium concentration $c_{eq} = 0$ for simplicity). The reaction kinetics are expected to be close to zeroth order for moderate to high pH values under conditions far from equilibrium (Wood and Walther 1983). Close to equilibrium a parabolic or higher order law ($n = 2 - 3$) is more likely (Lasaga 1986). The maximum velocity V is equal to V_0 when $c = 1$. As $c_s\ (t) = Kc_0(t) = KB_{1/2}(t\ )$, in practice, for the situations mentioned above, the position can be calculated as $x = \int_0^t V(t')dt' = V_o\int_0^t [B_{1/2}\ (t')]^n dt'$. Width measurements of the resulting zonation patterns show that H decreases insignificantly with n (~ 0.03 from $n = 0$ to $n = 3$). The valve ξ is insensitive to the choice of n. Consequently, a time-dependent velocity does not change the statistics of the zoning pattern when measured by Equation 3.

Discussion

The data presented here show that self-affine fractal geometry can be used to characterize zoning patterns. Sometimes, the scaling extends over two decades; in other cases curved log-log plots suggest a crossover between two fractal regimes or more complex behavior. The observed Hurst exponents, which are mostly between 0.25 and 0.45, indicate that the zonation is anti-persistent (the increments are negatively correlated). Halden and Hawthorne (1993) used the gray level of cathodoluminescence images of zircon as a subject for power spectra analysis. Hurst exponents in the range 0.34–0.42 were found, which are similar to our observations. These results also imply that zoning patterns are different from most surfaces where H typically is between 0.65 and 0.80. Large jumps in composition were observed in the garnet and plagioclase profiles. This feature cannot be modeled as fBm since increments with large absolute value are improbable. The jumps must correspond to large scale events like the opening or sealing of veins in a hydrothermal system or sudden decompression of a magmatic system. For sufficiently large length or concentration scales, the effective Hurst exponent tends toward zero because there is a limit to the concentration range. This was observed in some zoning patterns (e.g., GB and K92−2b in Fig. 7 and V2a and V2b in Fig. 4). Hurst exponents measured in this limit should be interpreted as a result of crossover phenomena rather than fractal scaling.

The most probable explanation for the apparent antipersistent behavior is that the input noise itself is antipersistent. It is possible to construct a growth model in which a period of increase in concentration, is more likely to be followed by a decrease in concentration, and vice versa. It is more difficult to construct a model in which the correlations in the zoning patterns are independent of any length scale like L and D/V, which is a requirement for fractal behavior. Consequently, it is difficult to explain the statistics of the zoning patterns in terms of internal processes. Variation in the environment, for instance temperature, oxygen fugacity, pressure, and pH, also contributes to the external forcing. As the compositions of hydrothermal garnets are very sensitive to these changes (Jamtveit et al. 1995), these parameters may have an equally strong effect on the zonation as do the variations in the major components in the fluid. Both plagioclase crystals analyzed here originated from samples that show evidence for magma mixing in their source regions (Gardner et al. 1995; Francis et al. 1989). In addition, the fluctuations in magmatic H_2O content, temperature, and storage depth have all played a part in controlling the plagioclase zoning patterns at Mount St. Helens (Gardner et al. 1995). It is an open question as to whether our plagioclase crystals are representative. Our zoned crystals are different from the ones studied by Pearce and Kolisnik (1990).

Adding white noise ($1/f^0$ noise) to a Brownian motion curve ($1/f^2$ noise) results in effective Hurst exponents that are lower than 0.5. Because experimental error noise often is simular to white noise, the presence of experimental noise may lead to an underestimation of Hurst exponents. We have tested this numerically by adding fBm and white noise, and we found that the Hurst exponent is underestimated by about 0.10 for the vesuvianite data, assuming that the experimental noise is white noise.

Hurst exponents measured from power spectra agree to some extent with the exponents measured from the width, but the uncertainty was, in some cases, very large. Attempts were also made to find periodic components of

the zoning patterns using power spectra. The high noise level in the power spectra made this difficult, and no distinct indication of periodic oscillation was found. The nonperiodic behavior was also confirmed by the difference between our results and a width measurement of a periodic pattern. The period of oscillation of a periodic pattern corresponds to a length $l_{p.}$ For $l \ll l_p$the width measurement gives a slope (in a log-log plot) that is close to one. For $l \gg l_{p,}$ the slope is close to zero. The details of the crossover region, where $l \simeq l_p$ depend on the exact shape of the periodic pattern. A more complex pattern will in general be associated with a wider crossover region. Periodic or quasi-periodic patterns are qualitatively different from fractal patterns that have no characteristic length scales.

The main result from the simulations is that the zoning patterns mostly reflect an external fluctuation in open systems. In a porous medium, diffusion processes can dampen the external fluctuation to some extent. Therefore, the presence of zonation indicates growth conditions where diffusion did not play an important role in wiping out concentration gradients. An interface-concentration-dependent growth velocity does not change the power law statistics. If the solid composition (c_s) is a multi-valued function of the fluid composition (c_0) (Wang and Wu 1995; Ortoleva 1994; Haase et al. 1980), the characteristics of the input noise may be severely changed by the growth process. This may occur for minerals with highly non-ideal solid solution. Large jumps in solid composition will occur whenever the input noise $c_0(t)$ reaches certain threshold values. Noise-induced transitions are thus possible in such systems.

Recently, several geological patterns have been explained by self-organization (Ortoleva 1994). For closed systems, like polycrystalline agate, it is likely that zonation is caused by internal processes (Ortoleva et al. 1994; Wang and Merino 1995). Several models have been published that also show that oscillatory zonation of minerals may be caused by nonlinear feedback processes. These models assume that the environment in which the crystals are growing is kept constant. A question of key importance is whether these models can describe naturally zoned crystals. If the geological environment changes on time scales that are small compared to the period of oscillation predicted by these models, detection of periodic components in the zonation patterns is difficult. With the many processes that govern crystal growth, there is also a possibility that some natural zonation patterns are caused by chaotic behavior. Periodic changes in fluid composition can lead to chaotic patterns in immiscible solids (Jamtveit 1991). All zoning patterns presented in this paper were tested for chaotic behavior by the Grossberger-Procaccia method (Grossberger and Procaccia 1983) and nonlinear forecasting (Sugihara and May 1990), always with a negative result.

Acknowledgments

We thank Turid Winje (University of Oslo) for assistance during the SEM work. The Mount St. Helens plagioclase sample was donated by David Pyle, University of Cambridge, and the Cerro Galan sample by Steve Sparks, University of Bristol. Geoff Grime is thanked for his help with PIXE analysis. This work has received support from The Norwegian Research Council (NFR) (Program for Supercomputing). This study is part of the Ph.D. work of T.H. and is supported by grants no. 440.94/003 and 440.95/006 from NFR.

References cited

Allegre, C.J., Provost, A., and Jaupart, C. (1987) A discussion of PIXAN and PIXANPC - the AAEC PIXE analysis computer packages. Nuclear Instruments and Methods, B22, 64–67.

Criswell, C.W. (1987) Chronology and pyroclastic stratigraphy of the May 18, 1980, eruption of Mount St. Helens, Washington. Journal of Geophysical Research, 92, 10237–10266.

Feder, J. (1988) Fractals, 283 p. Plenum Press, New York.

Francis, P.W., Sparks, R.S.J., Hawkesworth, C.J., Thorpe, R.S., Pyle, D.M., Tait, S.R., Mantovani, M.S., and McDermott, F. (1989) Petrology and geochemistry of volcanic rocks of the Cerro Galan caldera, northwest Argentina. Geological Magazine, 126, 515–547.

Gardner, J.E., Carey, S., Rutherford, M., and Sigurdsson, H. (1995) Petrologic diversity in Mount St. Helens dacites during the last 4000 years: implications for magma mixing. contributions to Mineralogy and Petrology, 119, 224–238.

Goldschmidt, V.M. (1911) Die Kontaktmetamorphose im Kristianiagebeit, 405 p. Skrifter fra det Norske Vitenskaps Akademi, Oslo, Matematisk Naturvitenskapelig Kl.11.

Grossberger, P. and Procaccia, I. (1983) Measuring the strangeness of strange attractors. Physica D, 9, 189–208.

Haase, C.S., Chadam, J., Feinn, D., and Ortoleva, P. (1980) Oscillatory zoning in plagioclase feldspar. Science, 209, 272–274.

Halden, N.M. and Hawthorne, F.C. (1993) The fractal geometry of oscillatory zoning in crystals: Application to zircon. American Mineralogist, 78, 1113–1116.

Jamtveit, B., (1991) Oscillatory zonation patterns in hydrothermal grossular-andradite garnet: Nonlinear dynamics in regions of immiscibility. American Mineralogist, 76, 1319–1327.

Jamtveit, B. and Andersen, T. (1992) Morphological instabilities during rapid growth of metamorphic garnets. Physics and Chemistry of Minerals, 19, 176–184.

Jamtveit, B. and Hervig, R.L. (1994) Constraints on transport and kinetics in hydrothermal system from zoned garnet crystals. Science, 263, 505–508.

Jamtveit, B., Wogelius, R.A., and Fraser, D.G. (1993) Zonation patterns of skarn garnets: Records of hydrothermal system evolution. Geology, 21, 113–116.

Jamtveit, B., Ragnarsdottir, K.V., and Wood, B.J. (1995) On the origin of zoned grossular-andradite garnets in hydrothermal systems. European Journal of Mineralogy, 7, 1399–1410.

Jamtveit, B., Grorud, H.F., and Ragnarsdottir, K.V. (1996). Flow and transport during contact metamorphism and hydrothermal activity: An example from the Oslo Rift. In B. Jamtveit, and B.Yardley, Eds., Fluid flow and transport in rocks. Chapman and Hall, London.

Kirkpatrick, R.J., Klein, L., Uhlmann, D.R., and Hays, J.F. (1979) Rates and processes of crystal growth in the system anorthite-albite. Journal of Geophysical Research, 84, 3671–3676.

Klug, C. and Cashman, K.V. (1994) Vesiculation of May 18, 1980, Mount St. Helens magma. Geology, 22, 468–472.

Lasaga, A.C. (1982) Toward a master equation in crystal growth. American Journal of Science, 282, 1264–1288.

———(1986) Metamorphic reaction rate laws and development of isograds. Mineralogical Magazine, 50, 359–373.

L'Heureux, I. (1993) Oscillatory zoning in crystal growth: A constitutional undercooling mechanism. Physical Review E, 48, 4460–4469.

L'Heureux, I. and Fowler, A.D. (1994) A nonlinear dynamical model of oscillatory zoning in plagioclase. American Mineralogist, 79, 885–891.

Mandelbrot, B.B. (1982) The fractal geometry of nature, 468 p. W.H. Freeman, San Francisco, California.

———(1985) Self-affine fractals and fractal dimension. Physica Scripta, 32, 25–260.

Meakin, P. (1997) Fractals, scaling and growth far from equilibrium, Cambridge University Press, Cambridge, U.K., in press.
Muan, A. (1979). Crystallization in silicate systems. In H.S. Yoder, Ed., Evolution of the igneous rocks, p.77–132. Princeton University Press, Princeton, New Jersey.
Ortoleva, P. (1990) Role of attachment kinetic feedback in the oscillatory zoning of crystals grown from melts. Earth Science Reviews, 29, 3–8.
———(1994) Geochemical self-organization, 411 p. Oxford University Press, New York.
Ortoleva, P., Chen, Y., and Chen, W. (1994). Agates, geodes, concretions and orbicules: Self-organized zoning and morphology. In J.H. Kruhl, Ed., Fractals and dynamic systems in geoscience, 421 p. Springer-Verlag, Berlin.
Pearce, T.H. and Kolisnik, A.M. (1990) Observations of plagioclase zoning using interference imaging. Earth-Science Reviews, 29, 9–26.
Peitgen, H.O. and Saupe, D., Eds. (1988) The science of fractal images, 312 p. Springer-Verlag, New York.
Rutherford, M.J., Sigurdson, H., Carey, S., and Davis, A. (1985) The May 18, 1980, eruption of Mount St. Helens 1. Melt composition and experimental phase equilibria. Journal of Geophysical Research, 90, 2929–2947.
Shore, M. and Fowler, A.D. (1997) Oscillatory zoning in minerals: A common phenomenon. Canadian Mineralogist, in press.
Simakin, A.G. (1983) A simple quantitative model for rhythmic zoning in crystals. Geokhimiya, 12, 1720–1729.
Sugihara, G. and May, R.M. (1990) Nonlinear forecasting as a way of distinguishing chaos from measurement error in time series. Nature, 344, 734–741.
Valley, J.W., Peacor, D.R., Bowman, J.R., Essene, E.J., and Allard, M.J. (1985) Crystal chemistry of a Mg-vesuvianite and implications of phase equilibria in the system CaO-MgO-Al_2O_3-SiO_2-H_2O-CO_2. Journal of Metamorphic Geology, 3, 137–153.
Voss, R.F. (1986) Characterization and measurement of random fractals. Physica Scripta, T13, 27–32.
Wang, Y. and Merino, E. (1992) Dynamic model of oscillatory zoning of trace elements in calcite: Double layer, inhibition, and self-organization. Geochimica et Cosmochimica Acta, 56, 587–596.
———(1995) Origin of fibrosity and banding in agates from flood basalts. American Journal of Science, 295, 49–77.
Wang, J.-H. and Wu, J.-P. (1995) Oscillatory zonation of minerals and self-organization in silicate solid-solution systems: a new nonlinear dynamic model. European Journal of Mineralogy, 7, 1089-1100
Wood, B.J. and Walther, J.V. (1983) Rates of hydrothermal reactions. Science, 222, 413–415.
Yardley, B.W.D., Rochelle, C.A., Barnicoat, A.C., and Lloyd, G.E. (1991) Oscillatory zoning in metamorphic minerals: an indicator of infiltration metasomatism. Mineralogical Magazine, 55, 357–365.

Manuscript received June 28, 1996
Manuscript accepted January 24, 1997

Appendix 1: sample descriptions and geological settings

Vesuvianite

The analyzed vesuvianite was from a carbonate-rich roof pendant near the western margin of the Eikern alkali-granite in the Oslo Rift, southern Norway. The locality was referred to as the Hamrefjell locality in the classical work of Goldschmidt (1911) [see Jamtveit et al. (1996), for a brief description of the contact aureole around this granite]. The vesuvianite occurs as milimeter- to centimeter-sized, yellow, euhedral crystals grown on the contacts between carbonate and shale layers. The vesuvianite-bearing mineral assemblage consists of grandite garnet, clinopyroxene (diopside-hedenbergite), calcite, and titanite. This mineral assemblage crystallized in the presence of very H_2O-rich pore fluids (Valley et al. 1995), consistent with infiltration of magmatic fluids in highly porous layers near shale-carbonate contacts (Jamtveit et al. 1995) at temperatures > 400 °C.

Garnets

All analyzed garnets were hydrothermal grossular-andradite garnets grown within contact aureoles around silicic to intermediate intrusives in the Permian Oslo Rift, south Norway. The complexly zoned garnets and the contact metamorphic setting were previously described in a series of papers by Jamtveit and coworkers (Jamtveit 1991; Jamtveit and Andersen 1992; Jamtveit et al. 1993; Jamtveit and Hervig 1994; Jamtveit et al. 1995). Intracrystalline compositional variations were observed with respect to the major components Fe^{3+}, Al, Mn, and Ti as well as the trace elements As, W, F, and rare earth elements (REE), and oxygen isotope composition. The zonation was generally concentric, but sector and intrasectoral zonation have occasionally been observed (Jamtveit et al. 1995). Large amplitude variations in core-to-rim compositional profiles have been interpreted as a direct result of variable fluid-flow rates in a hydrothermal system with significant kinetic dispersion control on the mass transport. In other words, the major features of the zonation profiles are thought to result from the competition between external (infiltration) and internal (local) controls on the pore fluid composition at the site of crystal growth. External fluids are dominantly magmatic, but a significant meteoric component seems to be present during growth of andradite-rich garnets (Jamtveit and Hervig 1994).

Plagioclase

Sample SH80-D is a gray dacite pumice from the Plinian phase of the May 18th, 1980, eruption of Mount St Helens. The sample comprises 31 vol% phenocrysts of amphibole (2%), plagioclase (24%), orthopyroxene (4%), and iron-titanium oxides (1%) set in a vesicular glassy matrix containing abundant microlites of plagioclase (An_{18-35}), orthopyroxene, and oxides. The microcrystalline nature of the groundmass, replacement of amphibole, and gray color distinguish SH80-D from the more abundant white dacite pumice of the Plinian phase (Criswell 1987). Similar gray pumices do, however, characterize the initial blast deposit of the May 1980 eruption. It is probable that SH80-D is vestigial cryptodome material entrained by deeper dacitic magma during the Plinian phase (Klug and Cashman 1994). Consequently the phenocryst phases in SH80-D record earlier crystallization in the MSH magma chamber at pressures of ~220 MPa (Rutherford et al. 1985). Coexisting Fe-Ti oxide phenocrysts from SH80-D record temperatures of 922 ± 13 °C at $\log_{o2} = -10.6 \pm 0.2$. The analyzed grain is 0.5×0.7 mm in size and comprises a patchy subhedral core containing several glass inclusions surrounded by an oscillatory-zoned mantle (An_{37-75}), with at least three resorption surfaces.

Sample SS40 originates from a porphyritic rhyodacite lava from the 4.2 Ma Real Grande ignimbrite eruption of

Cerro Galan caldera complex, northwest Argentina (Francis et al. 1989). It comprises 28% phenocrysts of plagioclase (17%), quartz (1%), biotite (6%), amphibole (2%) and irono-titanium oxides (2%) in a glassy nonvesicular matrix. Some amphiboles have thin orthopyroxene rinds. Plagioclase zoning is ubiquitous, typically consisting of a small resorbed andesine core (An_{40}) with a broad oscillatory-zoned mantle (An_{32-40}) and a thin outer rim of An_{48-50}. The analyzed crystal is 3.7 × 1.6 mm in size and lacks a discernible calcic core. Coexisting iron-titanium oxide phenocrysts indicate equilibration temperatures of 820 ± 40 °C at $\log_{o2} = -11.9 \pm 0.5$ (Francis et al. 1989).

Appendix 2: analytical methods

Microphotographs of vesuvianite samples were digitized using a Nikon LS 3500 film scanner. The BSE images of garnets were photographed on 60 mm negatives, which were digitized onto a Kodak Photo-CD. Black and white films were used. All photographs were digitized with a resolution of 2000 × 3000 pixels. The digitized pictures were first aligned with stripes of equal grayscale in the horizontal direction. The zoning profile was then obtained by measuring the light intensity in the vertical direction (the crystal growth direction). An average was made over 10 pixels (~10 μm) in the horizontal direction. The photographs were taken with as much contrast as possible, covering most of the grayscale range from 0 to 255. The grayscale in the digitized image is proportional to the logarithm of the light intensity. The sections used for analysis did not contain cracks, resorbed surfaces, or surfaces with morphological instabilities.

Electron microprobe (EMP) analysis of major elements was done on the CAMECA CAMEBAX microprobe at the Mineralogical Geological Museum, University of Oslo, and on the JEOL JXA-8600 Superprobe at the Department of Geology, University of Bristol, using 15 keV electrons, 20 nA operating current (40 nA for plagioclase), ZAF data reduction, and 1–2 μm diameter beam. The experimental error associated with the Ti content of vesuvianite was about 0.06 wt%. The spatial resolution was invariably near the maximum possible resolution (except for V1a), i.e., in the range 2–10 μm. For the plagioclase measurement, the 2σ precision based on counting statistics is < 1.5% relative for Al, Si, and Ca, 2.5% for Na, and 4% for K.

PIXE analysis was performed on 60 μm ''thick'' sections using the Scanning Proton Microprobe facility at the Department of Nuclear Physics, University of Oxford, with 3 MeV protons focused to a 1 μm spot and a mean sample current of ~ 0.3 nA. Energy-dispersive X-ray analysis was conducted on a SiLi detector with Be window and a 1 mm perspex filter to attenuate low-energy major element X-rays. The beam was scanned along a 400 μm line, with data collected in 256 bins, for a total analysis time of 300 min. X-ray yields and backgrounds were calculated using PIXAN software (Clayton et al. 1987) applied to the entire scan and then used to convert raw counts to parts-per-million units for each bin. The PIXE data were normalized to the Ca content of the centerpoint of the scan based on EMP analysis of the identical point. Difficulty in precisely matching the EMP analysis and scan centerpoint introduces a potential error of 10% relative, which is considerably greater than the statistical precision (4%) for Ca. The anorthite mole fraction was determined from Ca content alone. For Ca, 90% of the X-ray signal is derived from the top 14μm of the sample.